Analysis of the lightning activity during 18 years in the Congo Basin

Jean Kasereka Kigotsi, Serge Soula, Gilles Athier, Louis Kongoda Lisika, Keun-Ok Lee

Atmospheric Research 309 (2024) 107577

Contents lists available at ScienceDirect

Atmospheric Research

journal homepage: www.elsevier.com/locate/atmosres

Analysis of the lightning activity during 18 years in the Congo Basin

Jean Kasereka Kigotsi [a], Serge Soula [b,*], Gilles Athier [b], Louis Kongoda Lisika [a], Keun-Ok Lee [c]

[a] Faculté des Sciences et Technologies, Mention Physique et Technologie, Université de Kinshasa, Kinshasa, République Démocratique du Congo
[b] Laboratoire d'Aérologie, Université de Toulouse, UT3, CNRS, IRD, Toulouse, France
[c] Laboratoire de L'Atmosphère et des Cyclones, UMR 8105, CNRS, Université de La Réunion, Météo-France, Saint-Denis, France

ARTICLE INFO

Keywords:
Congo basin
Lightning activity
Detection efficiency
Multiplicity
Lightning trend

ABSTRACT

Lightning activity over an 18-year period between 2005 and 2022 recorded by the World Wide Lightning Location Network (WWLLN) in a 25° × 25° area of the Congo Basin is analyzed. In addition, data from the Lightning Imager Sensor (LIS) is used: between 2005 and 2014 from the Tropical Rainfall Measuring Mission (TRMM) and between 2018 and 2022 from the International Space Station (ISS). This duration makes it possible to consider an examination of the climatological trend of lightning in a context of strong global warming. The interannual evolution of the lightning activity on a global scale and at different time and space scales shows that the number of lightning flashes detected is significantly correlated with the average multiplicity (determination coeffcient of 0.92). Thus, this evolution can be mainly explained by variations in the detection efficiency of the WWLLN network. The study area is divided into five zonal bands of 5° latitude and their contributions to the annual global lightning activity are analyzed over the whole period: (i) lightning activity increases in the two bands north of the equator; (ii) lightning activity shows small variations in the most active band south of the equator; (iii) lightning activity decreases in the two southernmost bands. The maximum proportion of lightning on the scale of the small areas (5° × 5°) is found in the first southern zonal band (between 5°S and 0°), entirely at the annual scale and in 60% of cases at the seasonal scale. In DJF and MAM, this proportion is near 100%, while it is more scattered in the two northern zonal bands in 94% of cases in JJA. The local maximum density of flashes is in the same area every year.

1. Introduction

Space observations show that the most lightning-struck place in the world is around the Lake Maracaibo in Venezuela (Albrecht et al., 2011, and Albrecht et al., 2016; https://www.futura-sciences.com). However, Africa occupies six places in the top ten of the world ranking of the lightning hotspots, having five of them in the Democratic Republic of Congo (DRC). It is notable that the lightning density observed in the Lake Maracaibo region is highly localized with a spatial extension at <100 km both in the north-south and east-west directions (Burgesser et al., 2012). On the other hand, the primary and sharp maximum of flash density found in the Congo Basin has an extension of about 300 km in the north-south direction and 200 km in the east-west direction (Soula et al., 2016). Furthermore, a secondary maximum is observed in the Congo Basin, without well-defined size, geographic boundaries and contrast compared to the primary maximum (Kigotsi et al., 2018). The largest lightning densities in the world, concerning areas of significant dimensions, are thus found on the DRC territory (Williams and Stanfill, 2002; Christian et al., 2003; Cecil et al., 2014; Albrecht et al., 2016). In the study by Soula et al. (2016), the contrast between the regions of the primary and secondary lightning activity maximum changed during the 9-year period from 2005 to 2013.

The maps of lightning density in Soula et al. (2016) allowed to associate ground features, as the Virunga Mountains and a few lakes, with large values of the lightning density. However their study is limited to associate lightning activity with factors characterizing the atmospheric dynamics and thermodynamics in the region. A recent study (Kigotsi et al., 2022) reported an evidence of the contribution of a large number of lakes in the Lake Upemba region. Similarly, the roles of the Virunga mountains and lakes Kivu, Victoria and Tanganyika in increasing the lightning activity have been mentioned in some works (Laing et al., 2011; Soula et al., 2016). Moreover, the roles of orography and lake breezes in the thunderstorm development and the lightning distribution have been reported in several previous works around the world (Oki and Musiake, 1994; Hodanish et al., 1997; Yang and Slingo, 2001; Pujol et al., 2005; Antonescu and Burcea, 2010). Nevertheless,

* Corresponding author.
E-mail address: serge.soula@aero.obs-mip.fr (S. Soula).

https://doi.org/10.1016/j.atmosres.2024.107577
Received 19 December 2023; Received in revised form 4 July 2024; Accepted 6 July 2024
Available online 8 July 2024

several factors associated with the large-scale atmospheric circulation may contribute to the contrasting spatial distributions of flashes in the Congo Basin, e.g., the atmospheric equatorial Kelvin waves modulating the convection activity in equatorial Africa (Laing et al., 2011). They can modify the zonal distribution of lightning proportions in the study area in accordance with their properties: the maximum signal locates at the equator; but then, their amplitude is reduced by 50% at 6.5°N latitude and becomes zero beyond 13°N (Wheeler and Kiladis, 1999; Wheeler et al., 2000). In addition, they can also affect the meridian distribution of lightning properties depending on the spatial location of their source because of their meridional propagation from central Africa and/or the Atlantic Ocean to the Indian Ocean (Laing et al., 2011).

Seasonal singularities involving wind shear or convergence associated with the East African Jet (AEJ-S) may also represent as contrast factors. Jackson et al. (2009) found that in MAM (March, April, and May) during the period 2000–2003, the peak of the wind shear at 925 hPa level was located in the center of the Congo. Deep convection is however often associated with maximum wind shear in the 925–600 hPa layer of the troposphere (Laing et al., 2008; Mohr and Thorncroft, 2006). Moreover, a previous study showed the coincidence between the maximum lightning flash rate and the maximum convergence in the middle troposphere (600 hPa) around 25–30°E, in equatorial Africa, during the months of October of the period 1998–2003 (Jackson et al., 2009). It has also been shown that this convergence maximum coincides with the remarkable maximum in the number of mesocale convective systems (MCSs) in SON (September, October, and November) when the AEJ-S creator of this convergence is well developed (Jackson et al., 2009). The thunderstorms propagation from east to west in equatorial Africa is certainly one of the main factors in flash distributions (Nguyen and Duvel, 2008; Laing et al., 2011). During their propagation in this region, thunderstorms cover an average of 673 km (Laing et al., 2011). Therefore, the location of the convection initiation and the movement of the thunderstorms can influence the distribution of the lightning strikes throughout the study area.

The previous studies of lightning activity in the Congo Basin using the World Wide Lightning Location Network (WWLLN) data over 9 years from 2005 to 2013 (Soula et al., 2016; Kigotsi et al., 2018). The period was entirely covered by the Lightning Imager Sensor (LIS) onboard the Tropical Rainfall Measuring Mission (TRMM). LIS data revealed a relatively constant activity in both space and time for the study area and period (Soula et al., 2016). On the contrary, WWLLN data showed an increasing in yearly number of detected flashes, which suggested an increase of its detection efficiency (DE_W). It is worth extending the data beyond 2013 with a new series of 9-years WWLLN data (2014–2022) and 5-years LIS data (2018–2022) available thanks to the LIS on the International Space Station (ISS). The ISS/LIS, installed in February 2017, provides data on optically signatures of lightning flashes since the 1st March 2017 in an Earth area of ±55° of latitude (Blakeslee et al., 2020). The long series of optical transient detector (OTD)/LIS and WWLLN databases, covering almost two decades, now allow the investigation on the trends of lightning activity. For example, Qie et al. (2020) analyzed the trend of the lightning flash density in the tropics and subtropics based on 18 years of lightning data from 1996 to 2013 provided by the optical transient detector (OTD) and the TRMM/LIS. This study shows no significant trend for the flash density averaged over the study area, but significant trends at the regional scale in the sense of an increase or decrease. However, for the Central Africa which is the most active, the trend in relative values is less significant, especially for the period 1998–2013. In South Asia, the trend is clearly to an increase of the flash density (+0.096 flash km^{-2} $year^{-1}$ over the 2-decade period) due to various thermodynamic or microphysical factors according to the sub-region (Qie et al., 2021). By combining two sets of data, namely WWLLN on 2010–2019 and OTD/LIS on 1996–2013, Qie et al. (2022) showed a significant increase in lightning activity over the Tibetan Plateau, especially on its eastern part where it is most active.

The WWLLN Global Lightning Climatology (WGLC) was studied by Kaplan and Lau (2021) over a period of 16 years since the beginning of the WWLLN in 2005 and for the entire world. Interestingly, they found a DE_W increase at the global scale during the period of 2005–2013. They focused on the analysis for the second decade of the 21st century due to the reliability of dataset for investigating the spatio-temporal pattern of lightning and its changes. They noted a trend of increasing lightning activity in the tropics from 2012 to 2015 and in the midlatitudes of the northern hemisphere from 2016 to 2020. The present study is devoted to investigate the variability of lightning activity at various scales of time and space in the Congo basin for a longer period (to 2022) in the context of the climate change. The following sections of this paper are devoted to the methodology and data (Section 2), the results (Section 3), the discussion (Section 4) and the conclusion (Section 5).

2. Data and methodology

2.1. WWLLN data

The WWLLN data recorded during nine years (2005–2013) was analyzed in Soula et al. (2016) at various scales of time and of geographical distribution in the domain including the DRC and the Congo Basin, as same as used in the present study. The analysis period is extended to 2022 including the following 9 years (2014–2022) and thus making a 18-year period in total which is further representative for a climatology aspect and including the recent last eight years, which are also the warmest years on the Earth (2015–2022) according to the report of the World Meteorological Organization (World Meteorological Organization, 2023). The WWLLN (www.wwlln.net) is a global lightning detection network available since 2003. The sensors detect the electromagnetic radiations emitted by lightning strokes at very low frequency (VLF) and called sferics. If a stroke is detected by a sufficient number of sensors, it is localized thanks to the time of group arrival (TOGA) technique (Dowden et al., 2002). The stations can be separated by thousands of kilometers because VLF can propagate within the Earth-Ionosphere wave guide with little attenuation. With successive improvements in terms of number of stations and processing algorithms, the DE_W increased (Rodger et al., 2008). The WWLLN had for example >60 sensors in 2014. Both cloud-to-ground (CG) strokes and intracloud (IC) pulses of lightning flashes can be detected, but because they have larger peak current values, DE_W is better for the CG strokes as indicated by Bovalo et al. (2012). Abarca et al. (2010) showed that DE_W of the network was approximately 10% (35%) for strokes with a peak current larger than ±35 kA (−130 kA) by using the National Lightning Detection Network (NLDN). Thus, DE_W depends on the peak current and increases rapidly with its value. On the website of WWLLN it is now indicated the global DE_W is approximately 30% for strokes with peak currents around 30 kA and therefore probably lower for all strokes.

The WWLLN data can be used for purposes of lightning climatology (Bovalo et al., 2012; Soula et al., 2016; Kigotsi et al., 2018; Kaplan and Lau, 2021; Qie et al., 2022), physical processes related to convective activities in tropical cyclones (Abarca and Corbosiero, 2011; DeMaria et al., 2012), thunderstorm related to the production of gigantic jets (Soula et al., 2011), and the smoke effect of microphysics in thunderstorm (Altaratz et al., 2010). Because the flash is generally the metrics to characterize the lightning activity, the WWLLN events are associated in the same flash when they are separated by <20 km in distance and <0.5 s in time (Soula et al., 2016). Indeed, the sensitivity tests carried out on the distance criterion show a stabilization of the flash number when it exceeds 20 km, which suggests that the localization accuracy is clearly better than 20 km for the study area. The study considers the multiplicity, i.e. the number of detections (events) per flash. As it is observed from usual lightning detection networks, some strokes are duplicated in the sense where they are very close in time (generally <1 ms) and in space (variable distance). This aspect is checked and an analysis year by year shows several findings: (i) the duplicate strokes follow each other within 1 ms; (ii) most duplicate strokes are separated by <30 km, their

number stabilizes when the distance criterion between them exceeds 30 km; (iii) the percentage of duplicate strokes varies from <1% (2005 and 2008) to about 8% (2013 and 2014); they are eliminated by taking these criteria of time and space between them, i.e. 1 ms and 30 km.

2.2. LIS data

LIS is an optical sensor, initially onboard the scientific payload on the TRMM satellite (http://thunder.msfc.nasa.gov/lis/overview_lis_instrument.html), launched in December 1997 and ended in 2015 (Christian et al., 1999; Boccippio et al., 2002). It detects both IC and CG lightning flashes with an efficiency around 80% according to the time of the day (from around 70% at local noon to 88% during the night, as indicated in Cecil et al., 2014). TRMM had a 350 km orbit around the Earth and then 402 km after an orbit boost in August 2001. Soula et al. (2016) described the estimation of the proportion of the real flash number potentially detected by LIS, for a given area. Thus, with a 600 km × 600 km field-of-view, an inclination of 35°, allowing the coverage of the Earth between 38°N and 38°S, and by combining both the time and spatial coverages, they found that the TRMM/LIS could detect 0.124% of the flashes.

A new LIS has been installed onboard the ISS at an altitude of about 400 km in 2017, which allows us to have a new series of data starting in 2018 for complete years, i.e. five years. According to the larger inclination of the ISS orbits (about 51.6°), it covers a larger area of the Earth which is estimated to be between 55°S and 55°N in latitude with a DE around 60% (Blakeslee et al., 2020). In order to estimate the complete lightning activity within the study area, we use the method from Soula et al. (2016) which made an estimation of the time of exposure of any point of the area to the LIS. Two coefficients are calculated, α_t for the proportion of exposure time during an orbit which is the same as in Soula et al. (2016) because both LISs have the same altitude of 400 km and α_S for the proportion of the area of the Earth covered during one orbit compared to the total area covered by the set of the orbits which is the Earth surface between −55° and + 55° in latitude. Thus, α_t is about 1.61%. For the coefficient α_S it is different since the coverages of both LISs are not identical. For the ISS/LIS, we can estimate this coefficient with the method in Soula et al. (2016) and by taking into account the difference of coverage according to the latitude (regions in high latitudes have better coverage compared to that in low latitudes). It means the coverage is divided in two parts, one between −38° and + 38° to be consistent with Soula et al. (2016) and another one for the two bands, i.e. between −55° and − 38° in the south hemisphere and between 38° and 55° in the north hemisphere. Thus, α_S is found equal to 0.0515, i.e. 5.15%. The combination of both coefficients is therefore:

$$\alpha_L = \alpha_S \times \alpha_t = 8.29 \times 10^{-4} = 0.0829\%.$$

The number of flashes, $N_{L\ total}$, which could be detected by LIS with a geostationary orbit is evaluated by the number of flashes, N_L, detected by the ISS/LIS:

$$N_{L\ total} = \frac{N_L}{\alpha_L}$$

2.3. Methodology

The aim of this study is to characterize the spatial distribution of flashes in the Congo Basin and its evolution over a long period, especially including the recent hottest years on the Earth. A general trend for the whole study area is analyzed using the WWLLN data and the LIS data when it is available (for the whole period but three years). The number and proportion of flashes at various spatial scales are considered. Thus, the study region, highlighted by a blue square in Fig. 1 and defined by 15°S–10°N in latitude and 10°E–35°E in longitude, is divided in 25 squares with a 5° × 5° area. These square elements are named small areas and noted from area #1 to area #25 according to their location in the map of Fig. 1. As an example, area #1 corresponds to 5–10°N and 10–15°E. For the lightning flash activity within these small areas, we only use the data provided by the WWLLN. The number of flashes is

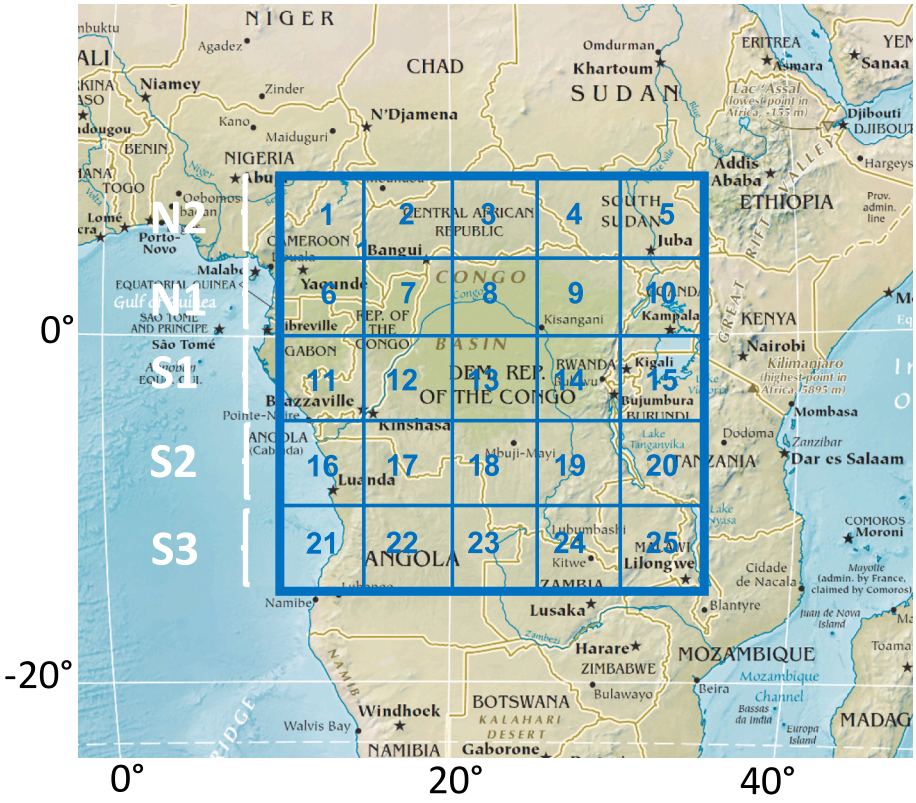

Fig. 1. Map of the study area within the African continent (large square) and different 5° × 5° areas (small areas from #1 to #25) used in the study of lighting activity trend during the period.

counted for each small area and an elementary statistical method is applied for calculating the proportions of lightning flashes thanks to an algorithm specifically designed. In the following, the proportion of flashes is calculated for a given area (small area or more) and a given duration (the whole 18-year period, the half period, one year, one season).

3. Results

3.1. Overall lightning activity during the period 2005–2022

Table 1 shows several parameters of the lightning activity retrieved from the two detection systems of WWLLN and LIS for 18 years period (except 2015–2017 without LIS data) and for the study area. The same parameters are plotted in the graph of time series in Fig. 2. All values for the period 2005–2013 are issued from Soula et al. (2016), except the multiplicity which is a little different because it is calculated by eliminating the duplicate strokes. N_W is the number of flashes retrieved from WWLLN (blue curve in Fig. 2). N_W increases between 2005 and 2014, having the largest value of 9,649,312 flashes in 2014. Then, N_W decreases substantially until 2018 to 6,369,679 flashes and increases again to 8673,959 flashes in 2022. While N_W shows an increasing trend during the whole first 9-year period, it shows two different trends during the second one. By comparing with LIS data, Soula et al. (2016) showed that the flash number increase from 2005 to 2013 was largely related to the improved DE. Unfortunately, the second period is not fully covered by LIS thus, it is limited to carry out the comparison analysis for entire period. The secondly-listed analysis parameter in Table 1 is the average annual multiplicity, M_m, for the flashes detected by WWLLN. Indeed, an improved DE for a lightning detection system can lead to a larger multiplicity, i.e. more strokes per flash in average (Rudlosky and Shea, 2013; Soula et al., 2016).

According to Table 1 and Fig. 2, N_W and M_m seem correlated. In order to quantify the correlation, we produce a scatter plot of two parameters (Fig. 3). For the whole study area (Fig. 3a), this correlation is highlighted with a high determination coefficient R^2 of 0.92 over the whole period (18 years). It indicates that the evolution of the flash numbers detected by WWLLN is largely due to the changes in DE. By separating the values in two periods, i.e., one up to 2014 when the flash number N_W reaches the maximum (blue dots) and another one after 2014 (orange dots), the determination coefficients are calculated to 0.93 and 0.90 for the first and second period, respectively. Two values are clearly below the regression line (blue dots) and probably degrade the correlation, corresponding to 2012 and 2013. The M_m value in 2013 (1.17) is the furthest from the regression line while the flash number, N_W, displays the strongest increase in the year (Fig. 2). Even if M_m increases between 2012 and 2013 (from 1.14 to 1.17), it stays below the trend curve, which means a better DE_W but not sufficient to explain the larger flash number N_W (an increase of 40%). It could probably support an increase of the lightning activity in 2013. On the other hand, the number of flashes from LIS N_L displays a clear increase between 2012 and 2013 which confirms an increase of the lightning activity. The same analysis can be carried out for the periods between 2013 and 2014: N_W increases by 5.1%, M_m substantially increases from 1.17 to 1.24 while N_L from LIS clearly decreases by 9.5%, which means the increase of the number of flashes detected by WWLLN is probably due to a better DE_W in spite of a decrease of the lightning activity (shown by LIS). After 2014, the multiplicity decreases slowly until 2017, then it varies little until the end of the period indicating a relatively constant DE. The N_W increase after 2018 means that the lightning activity could have increased during the last years of the period. However, N_L indicates a substantial decrease in 2022 which is not consistant with the other observations.

Fig. 3b is the scatter plots of M_m and N_W for each of the five zonal bands N2, N1, S1, S2 and S3 (see Fig. 1 for the zonal band identification). The distribution of the values for each zonal band is similar insofar the linear fitting has a high determination coefficient (from 0.84 to 0.94). Each band has a different slope which is reasonably related to its specific lightning activity, with S1 as the most active (green color) and S3 as the less active (red color). It shows that whatever the rate of lightning activity in the area, the number of flashes and the multiplicity can be highly correlated. It confirms that the number of flashes detected in the study area is strongly related to DE.

The ISS/LIS data only starts in 2018 and the number of flashes is substantially lower because of a different coverage, i.e., between ±38° in latitude for TRMM/LIS and ± 55° for ISS/LIS (Blakeslee et al., 2020). The ISS/LIS stays less time above the study area during one year. According to Soula et al. (2016), DE_W for WWLLN data can be estimated by using the number of flashes N_L detected by LIS. In Table 1, $N_{L\ total}$ represents the estimation of the flashes that would be detected by LIS with a continuous observation (see section 2.2). The values of $N_{L\ total}$ between 2018 and 2022 are very similar to those estimated for the period 2005–2014, except for year 2022 with a substantially lowered value. $N_{L\ total}$ has an average value of 1.497×10^8 with a low standard deviation of 0.073×10^8 (black dashed line in Fig. 2). From the values of $N_{L\ total}$, no trend is distinguished from the available data for the periods of 2005–2014 and 2018–2022. Finally, DE_W deduced from the number of flash $N_{L\ total}$ shows the increased value in 2014 with 6.86% and then lowered values after 2018, when the LIS flashes are available, mostly between 4 and 5% and then increased to 6.73% in 2022.

Fig. 4 shows the maps of the flash density (FD) from WWLLN for each year between 2014 and 2022 in the study area with a resolution of 0.1° × 0.1°. The same maps for the period of 2005–2013 are available in Soula et al. (2016). As in Table 1, it indicates a decrease of the annual maximum value of FD_M which is constantly in the eastern part of the study region. The maximum FD_M value is about 12.5 flashes km^{-2} in 2014 while it reduces to 4.3 flashes km^{-2} in 2018 (Table 1) which is a factor of about 3. The maximum value is consistent with the values found in previous studies based on total lightning activity from space (Albrecht et al., 2016). Indeed, with a DE_W of 6.86% that we have estimated for 2014, the value of the total flash density FD_M should be 182 flashes km^{-2} while the maximum value found in Albrecht et al. (2016) was 205 flashes km^{-2}. Not only the maximum value decreases over the first five years (2014–2018), but the region including the larger values of the lightning flash density, considered as the main maximum in Kigotsi et al. (2018), marks this drop of activity. On the contrary, the secondary region of large activity, more in the west and more spread out, decreases just a little or stays at the same level of density around 4 flashes km^{-2}. To summarize, the contrast between the main maximum

Table 1
For each year, N_W number of flashes from WWLLN, FD_M flash density maximum, M_m average multiplicity, N_L number of flashes from LIS, $N_{L\ total}$ number of flashes recovered from LIS, DE_W detection efficiency for WWLLN. (*adapted from Soula et al., 2016).

Year	N_W	FD_M (km^{-2} y^{-1})	M_m	N_L	$N_{L\ total}$	DE_W (%)
2005*	2,676,276	2.7	1.07	190,308	153,761,877	1.74
2006*	2,516,580	1.9	1.13	188,449	152,259,873	1.65
2007*	3,602,064	2.66	1.11	182,643	147,568,838	2.44
2008*	2,467,176	1.91	1.10	183,466	148,233,792	1.66
2009*	3,446,317	3.93	1.12	195,316	157,808,157	2.18
2010*	3,643,387	4.41	1.14	188,984	152,692,133	2.39
2011*	4,701,732	4.63	1.19	192,007	155,134,606	3.03
2012*	6,550,235	8.22	1.22	182,56	147,501,777	4.44
2013*	9,181,456	12.86	1.28	192,443	155,486,878	5.90
2014	9,649,312	12.47	1.07	174,165	140,718,925	7.13
2015	8,318,435	9.91	1.07	–	–	–
2016	7,083,318	7.97	1.09	–	–	–
2017	6,449,288	5.3	1.08	–	–	–
2018	6,369,679	4.32	1.10	127,351	153,620,024	4.15
2019	7,340,060	4.51	1.11	125,509	151,398,070	4.85
2020	6,809,147	5.77	1.12	120,834	145,758,745	4.67
2021	8,213,825	5.86	1.14	128,314	154,781,665	5.31
2022	8,673,959	5.76	1.17	106,816	128,849,216	6.73

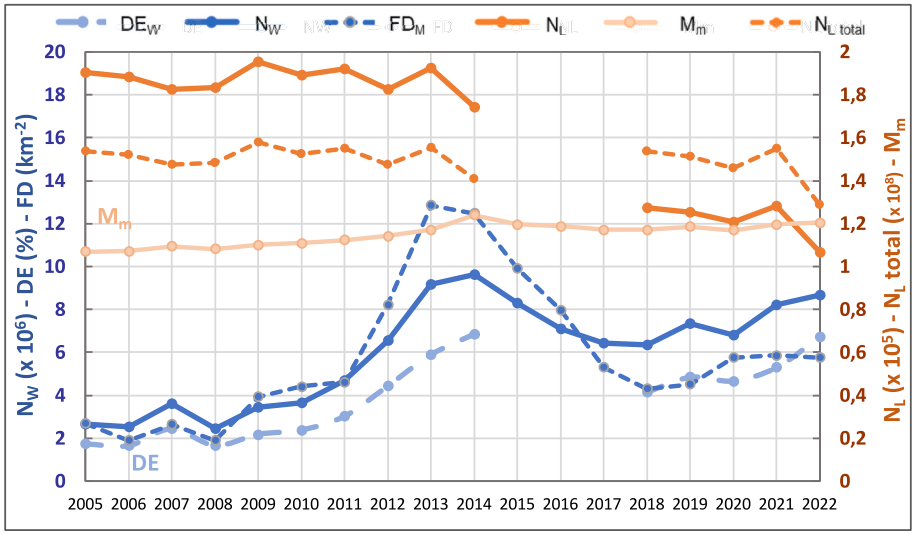

Fig. 2. Lightning flash activity within the study area from 2005 to 2022: time series of the lightning flash number, N_W (from WWLLN, blue curve) and N_L (from LIS, orange curve); the relative detection efficiency, DE (WWLLN versus LIS, dashed light blue curve); the average multiplicity, M_m (from WWLLN, light orange curve); the maximum flash density, FD (from WWLLN, dashed blue curve); the total flash number, $N_{L\ total}$ (from LIS, dashed orange curve with the average value indicated by a black dashed line). (For interpretation of the references to color in this figure legend, the reader is referred to the web version of this article.)

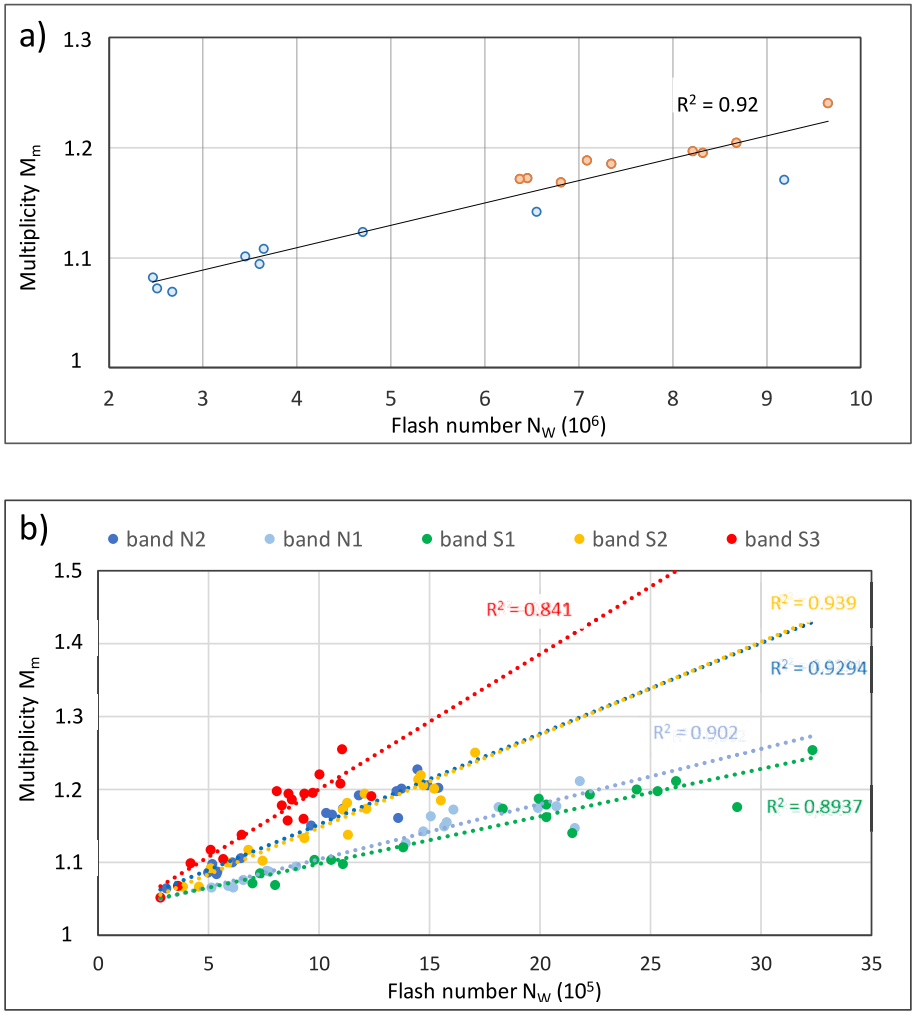

Fig. 3. Scatter plot of the annual number of flashes detected by WWLLN (N_W) and the annual average multiplicity (M_m) for 18 years: (a) for the whole area (blue dots for 2005–2014 and orange dots for 2015–2022), (b) for each zonal band (from north to south: N2, N1, S1, S2 and S3). (For interpretation of the references to color in this figure legend, the reader is referred to the web version of this article.)

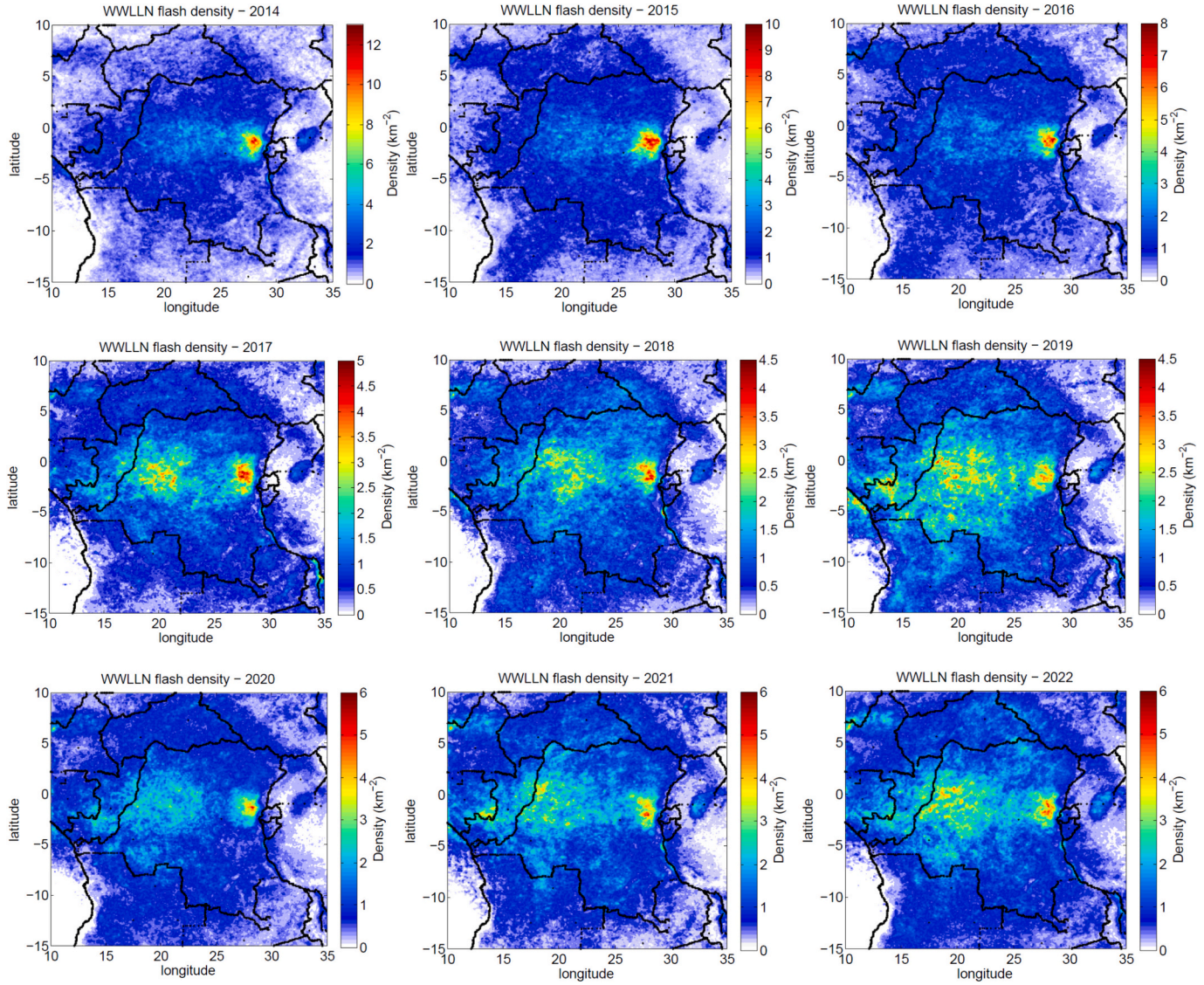

Fig. 4. WWLLN lightning flash density (flash km^{-2}) in the study area (10°E–35°E; 15°S–10°N) from 2014 to 2022. Resolution is 0.1° × 0.1° and the scale of the density is adapted for each graph with the maximum value.

and the rest of the study area decreases sharply in the second part of the 18-year period. The decrease of the lightning flash activity observed by WWLLN seems related to lower values of DE_W in the major region since it does not decrease when the LIS data are considered. However, it is difficult to figure out the trend over the three years of 2015–2017 using LIS data, but when they are available again in 2018, the number of flashes is 1.5×10^8 which is the average value over the whole period (2005–2022) for the whole study region. Such value for one year corresponds to 4.76 flashes per second which is about 11% of the flash rate estimated at 44 ± 5 lightning flashes per second for the whole Earth (Christian et al., 2003), while the study area S_A is only 1.5% of the total Earth area (λ and φ are the latitude and the longitude, respectively):

$$S_A = R_T^2 \int_{10^\circ}^{35^\circ} \int_{-15^\circ}^{10^\circ} cos\lambda \, d\lambda \, d\varphi$$

3.2. Spatio-temporal analysis of the annual lightning activity

Fig. 5a displays the proportion of lightning activity for each of the small 5° × 5° areas defined in Fig. 1, averaged over the whole period. At first glance, we note the near equality of the two largest average proportions associated with areas #13 and #14, 7.96% and 7.81%, respectively. The three larger values (areas #12, #13 and #14) are located in the zonal band S1 (5°S–0°) and represent 22.69% of the lightning flashes. The set of areas associated with values greater than or equal to 5% roughly determines the domain of large average proportions. The spatial configuration of this domain is identified with the zonal bands N1 and S1 (5°N–5°S) and the meridian band (10–30°E), from which area #6 (3.40%) must be subtracted and area #17 (5.11%) integrated (Fig. 5a). Therefore, this spatial configuration would coincide with the vast maximum in the number of MCSs characterizing active thunderstorms in equatorial Africa (Jackson et al., 2009). Moreover, this structure is, to a certain extent, compatible with the description of the two density maxima analyzed in Kigotsi et al. (2018). Indeed, area #14 encompasses the main maximum and the set formed by areas #11, #12, #13 and #17 determines a configuration compatible with the secondary maximum. In summary, we note, in accordance with this description, that the DRC territory presents the greatest average proportions of lightning, followed by the Republic of Congo, the southern half of Gabon and the northern sector from Angola (Fig. 5a). Moreover, we also observe that the average proportions of lightning are, each year, lower in the Rift Valley, east of the Virunga mountains in the meridian band (30–35°E) and in the western oceanic areas (#16 and #21).

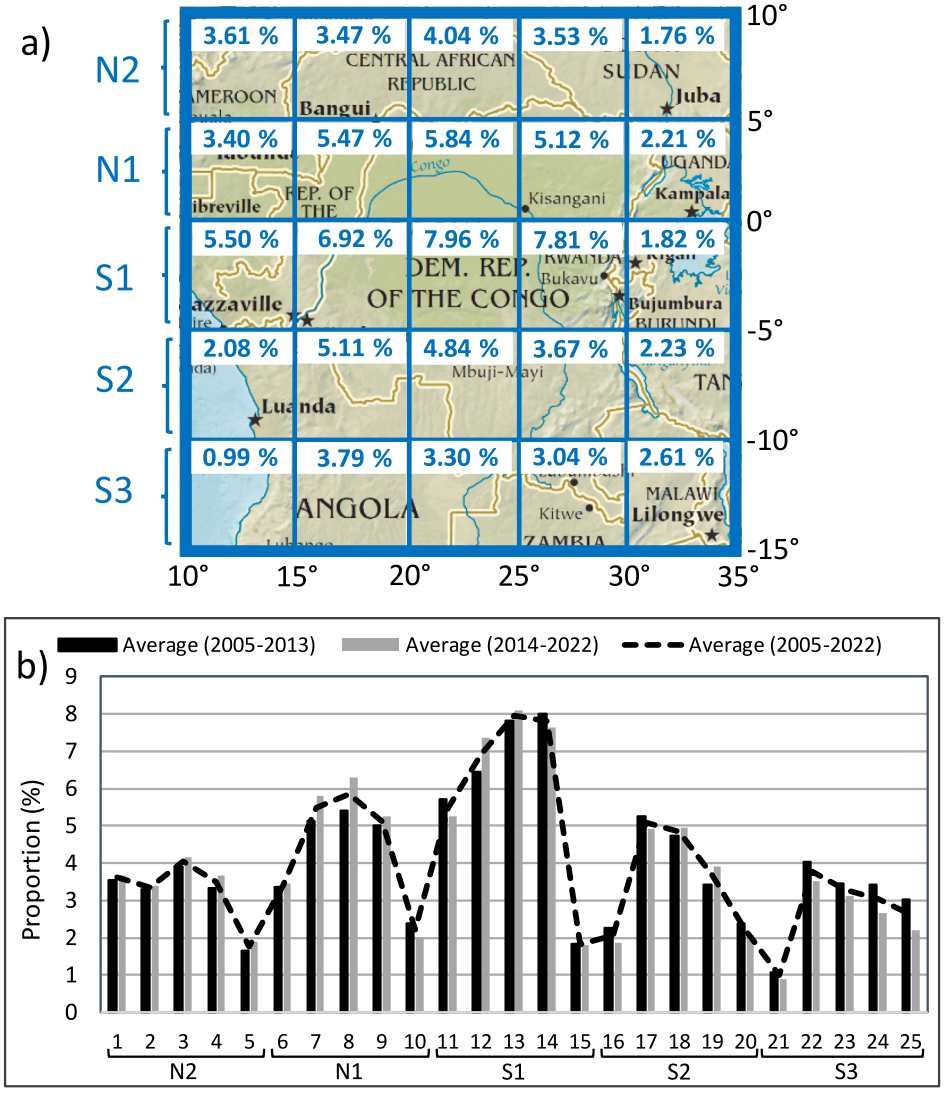

Fig. 5. a) Proportion of lightning flash activity for each small area and averaged over the whole period 2005–2022; b) The same proportions for the whole period and for two half periods.

Fig. 5b shows these proportions of lightning activity for three periods: the whole 18 years (2005–2022) and two half-periods (2005–2013 and 2014–2022), highlighting both zonal and meridian patterns. The third zonal band (areas #11 to #15) has the larger values, the two most northern and southern zonal bands have the lower values. In each zonal band, the larger values correspond with the central meridian band. This distribution is the same for both half-periods. For all small areas, the difference between both half-periods is not significant. However, there is a trend for slightly larger values in the second period (2014–2022) for areas in the two most northern zonal bands (areas #1 to #10) and the opposite trend for areas in the most southern band (areas #21 to #25).

The cumulative proportions of the five zonal bands from north to south (N_2, N_1, S_1, S_2, and S_3, respectively) are plotted in Fig. 6a and the average values over the whole period are indicated in Table 2, including the standard deviations. In a comprehensive way, the standard deviation values are low, ranging between 1.53% and 2.12%, however in relative they are lower for the central bands, especially for the most active band S1. In S1, the average proportion is highly close to 30%, which is also the values at the beginning and the end of the period, and the standard deviation is calculated to be 1.53% (ratio 5.10%). The proportion is more fluctuant in the most northern and southern bands, i.e., N2 and S3, with the standard deviation values of 1.94% (ratio 11.89%) and 2.12% (ratio 15.44%), respectively. Fig. 6a allows us to figure out the trend for each band. Decreasing proportion trends are found in the most southern bands (S2 and S3) whereas slight increasing trends are seen in the most northern ones (N1 and N2). The proportion trend in S1 is relatively constant during the period. Fig. 6b displays yearly-averaged multiplicity (M_m) for each zonal band. M_m evolves closely in all zonal bands while the largest values are often found in S3 (red color) which is also the least productive of lightning flashes. The lowest values are found mostly in N1 (just north to the equator) and furthermore its difference with other zonal bands increases during the last ten years (2013−2022), which indicates the relatively low DE_W in N1. Since the proportion of the lightning flashes tends to increase in this band (Fig. 6a), either it increases more than in the other bands, or it decreases less.

Fig. 7 displays the trend of the yearly lightning activity for each small area in five panels, i.e., one panel for each zonal band from north to south (i.e., from N2 to S3). The time series of the number of lightning flashes (N_W) for the whole study area (Fig. 2) are plotted in left panels while the proportion in flash (P_f) of each small area are displayed in right panels. Thus, the evolution for each area can be analyzed by both absolute and relative values. First, an N_W increase is observed in 2007, essentially in the areas of the three most southern bands (Fig. 7c, d, e), as in the whole area (Fig. 2). Since N_L (from LIS) does not exhibit this increase, it is due to a better DE_W for the southern part of the study area.

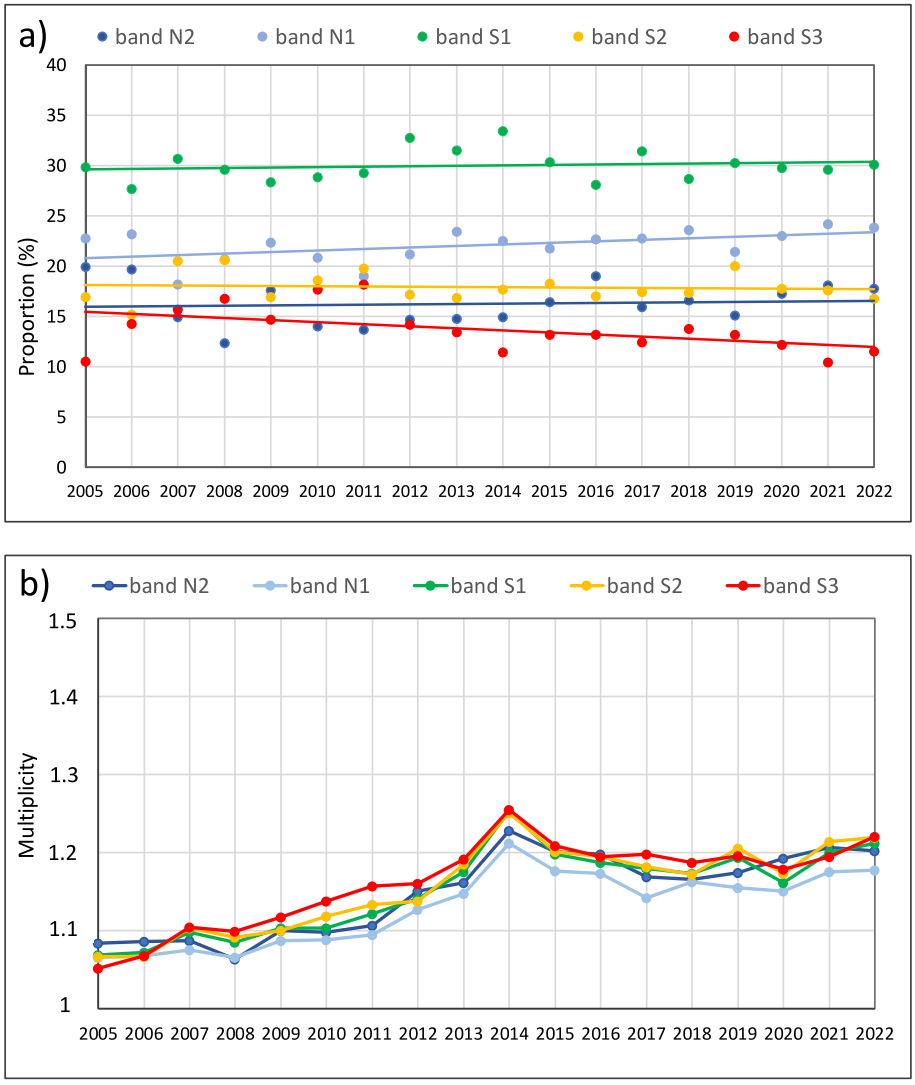

Fig. 6. Proportion of flashes (a) and average multiplicity (b) within the five zonal bands of the study area (from north to south: N2, N1, S1, S2 and S3) during a 18-year period. The lines in a) are the trend curves.

Table 2
Average proportion P_f, standard deviation SD and ratio between both in percentage, for the lightning flash number in each zonal band of the study area and over the whole period (2005–2022).

	Band N2 (5°N–10°N)	Band N1 (0°–5°N)	Band S1 (5°S–0°)	Band S2 (10°S–5°S)	Band S3 (15°S–10°S)
Average proportion P_f (%)	16.27	22.08	30.01	17.92	13.71
Standard deviation SD (%)	1.94	1.62	1.53	1.44	2.12
Ratio SD/P_f (%)	11.89	7.36	5.10	8.03	15.44

Simultaneously and in accordance, P_f decreases for the most northern bands (Fig. 7f, g). Then, N_W continues to increase in the most southern bands until 2013–2014 (Fig. 7d, e), susbtiantially after 2010. In the most northern bands, this increase begins around 2011 (Fig. 7a, b) and it is more pronounced in panels c and d with larger values for the most active areas (blue light, green and yellow curves in Fig. 7c, d). P_f changes a little during this period, especially in area #14 (Fig. 7h, yellow curve) from 6 to 10% which is the location of the main maximum of the lightning density (Fig. 4).

During the second period (2014–2022), there is a N_W decrease for a few years and in all areas, especially in the areas where there was a large increase previously. For the last years, the trend is rather to an increase for N_W. The largest P_f is seen in area #14 during a long period (2009–2016), and it finally decreases to 6% in 2022 which is only the third largest (Fig. 7h, yellow curve). The two largest values of P_f are found in areas #12 and #13 which corresponds with the secondary maximum in Kigotsi et al. (2018). Especially in the band N1 (Fig. 7g) and in the second period (2014–2022), P_f increases in the most western areas (#6, #7 and #8), which is consistent with Fig. 6b and the previous comments associated. This means that storm activity tends to spread more widely westward during the 2014–2022 period, as indicated by the flash density in Fig. 4. The most eastern areas (red curves in Fig. 7) exhibit mostly low proportions even in area #15 where Lake Victoria is located and exhibits a relatively-constant annual proportion of lightning flash of around 2% (Fig. 7h). In spite of a lightning "spot" over Lake Victoria, the rest of the area #15 is low in thunderstorm activity (Fig. 4).

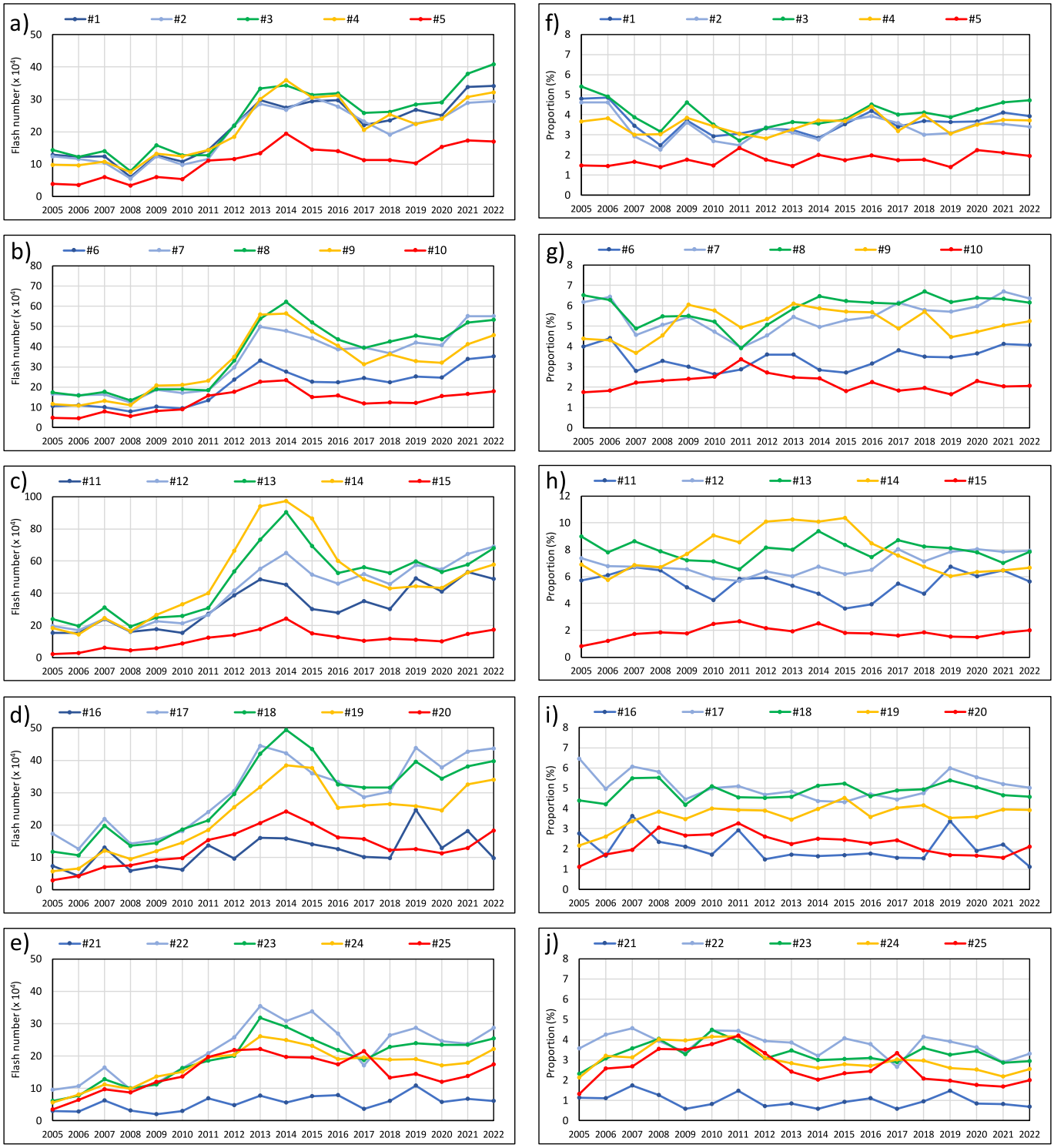

Fig. 7. Evolution over the 18 years of the flash number N_W (left panels) and the flash proportion P_f (right panels) in each area (#1 to #25). A panel corresponds with a zonal band (5 areas), a color with a meridian band (5 areas). The scale is adapted to the maximum value.

3.3. *Spatio-temporal analysis of the seasonal lightning activity*

The seasonal activity evolution is first analyzed over the 18-year period and in the whole area. Fig. 8 displays the number of flashes N_W detected by WWLLN for each season according to DJF (December, January and February), MAM (March, April and May), JJA (June, July and August) and SON. The first complete season is MAM 2005 and December 2005 is associated with DJF 2006. The overall evolution already observed for the annual flash number (Fig. 2) is observed for the seasonal periods as well. Thus, N_W exhibits an overall increasing trend during the first half-period (2005–2013) for all seasons, what appears to be related to an improved DE. In 2014, N_W significantly decreases only in SON season, which means the cause of this decrease starts at the end of 2014. Indeed, in 2014 the first season DJF corresponds to a large increase and the N_W increases are as well seen in both MAM and JJA seasons. Then, in 2015 all seasons correspond to a decrease of N_W.

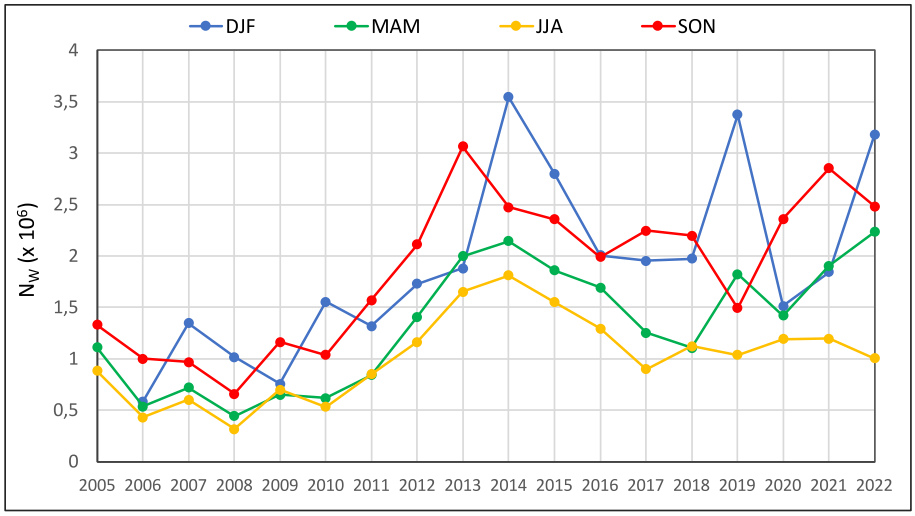

Fig. 8. Number of flashes from WWLLN for each season within the study area. The first complete season is MAM in 2005.

Another period corresponds to a decrease, where SON 2019, DJF 2020 and MAM 2020 chronologically indicate N_W drops. In general, the season SON (red curve) previously indicate the trend compared to the other seasons. The season DJF (blue curve) seems more fluctuant than the other seasons. This analysis by season allows us to distinguish more precisely the time of a change of trend.

The seasonal activity is now analyzed separately in the five zonal bands defined in Fig. 1 and Table 2 over the 18-year period. Fig. 9 shows the graphs for each band with the color code used in Fig. 8 for the seasons. The most sensitive seasons to the zonal bands are DJF and JJA with low activities in most northern (N2 in Fig. 9a) and most southern (S3 in Fig. 9e) bands, respectively. The lightning flash number seems to evolve alike in all zonal bands in MAM and SON (green and red curves, respectively) during the whole study period, with its own scale of value. In the zonal band S3 (Fig. 9e), flash numbers are contrasting in DJF and JJA (almost zero in JJA) but similar in MAM and SON. The decreases of LIS flashes oberved in 2014 (Fig. 2) and WWLLN flashes from the end of 2014 (SON and DJF in 2015 in Fig. 8) to the beginning of 2015 (DJF, blue curve in panels c, d) are found in all zonal bands (red curves in Fig. 9). The seasonal and zonal analysis allows us to show the existence of the decreasing phase that begins at the end of 2014 lasting about three years before it finally increases to the end of the period.

3.4. Seasonal location of flash proportion peaks

Table 3 and Table 4 display the areas with the maximum proportion of lightning flashes for each year and each season. The proportion is related to the total activity over the year, there are thus 71 seasons in total during 18 years (the first DJF season in 2005 is not complete). Out of the 71 values, the area #14 has the maximum value for 18 times (DJF, MAM and SON), the area #13 for 12 times (DJF, JJA and SON), the area #11 for 10 times (only MAM), the area #8 for 7 times (JJA and SON), the area #12 for 6 times (DJF and MAM), the areas #3 and #7 for 6 times each (JJA and SON). The other areas have therefore the maximum for 6 times. Fig. 10 summarizes the number of times that each small area has the seasonal maximum of the lightning flash number. We can note that the zonal band S1 has the maximum value 46 times during the period (65% of cases) and neither of the areas after the area #14 has a maximum value. The maximum value exceeds 4% two times, for area #14 during DJF in 2010 with 4.38% and during DJF in 2005 with 4.02%. The third value is also seen in area #14 with 3.90% during DJF in 2014. The larger values are found in DJF and MAM and the lower ones in JJA and SON. The three lower values correspond with JJA for different areas (#2, #7 and #9).

4. Discussion

This study extends and completes previous studies based on 9 years of lightning activity in a large region of the Congo Basin (Soula et al., 2016; Kigotsi et al., 2018), by doubling the data period and further detailing the trends by geographical area. Data is issued from the WWLLN for 18 years and from the LIS for two periods, one of 10 years from TRMM/LIS (2005–2014) and another one of 5 years from ISS/LIS (2018–2022). The overall trend of the yearly number of the lightning flashes detected by WWLLN (N_W) clearly follows that of the average multiplicity (M_m), in such a way both increase simultaneously. Indeed, the scatter plot displayed in Fig. 3 confirmed a high correlation between parameters with a determination coefficient equal to 0.92 for the linear curve fitting (correlation coefficient 0.96). The multiplicity is related to DE (Rudlosky and Shea, 2013), therefore it indicates that the N_W trend is mainly due to the DE_W evolution. Between 2005 and 2014, both values of N_W and DE_W increase except for a period between 2006 and 2008, and then they decrease until 2020 except for 2019 for N_W values, but increase again during two last years (Fig. 2). The increase during the first period 2005–2013 was strongly correlated with the number of stations and the improvement of the algorithms (Soula et al., 2016). It is implied that according to the low number of stations around the study area, the detection efficiency is highly sensitive to the stations status, especially if only one is faulty for a time period. Furthermore, during the study period, when the data was available, LIS detected a relatively constant annual number of flashes $N_{L\ total}$ estimated by taking into account its coverage coefficient, between 1.4 and 1.6 $\times$ 10^8 flashes. Thus, a change of the lightning activity at the scale of the study area is not visible during the 18-year period of which the eight last (2015 to 2022) are by far the hottest on Earth due to the global warming. Similarly, Kaplan and Lau (2021) analyzed WWLLN data from 2010 to 2019 and found an increase of the annual stroke number between 2010 and 2014 at Earth scale, and they explained also by a DE_W improvement. Then, the trend they observe looks like that of the present study with a decrease during 2014–2017, and a small increase during 2018–2019 followed by a decrease in 2020 (see their Fig. 2). In Kaplan and Lau (2021), the authors indicated more flashes in the tropics over the period of 2012–2015, it corresponds with the larger number of flashes in the present study but also wih the larger multiplicity values.

On the same way, a detailed analysis allows us to show that several observations support an increase of the lightning activity around 2013. Qie et al. (2020) found also an increase of the lightning activity in Central Africa from 2010 to 2013, last year of the LIS/OTD data set used in their study (see their Fig. 2e). Other consistencies are seen in the trend

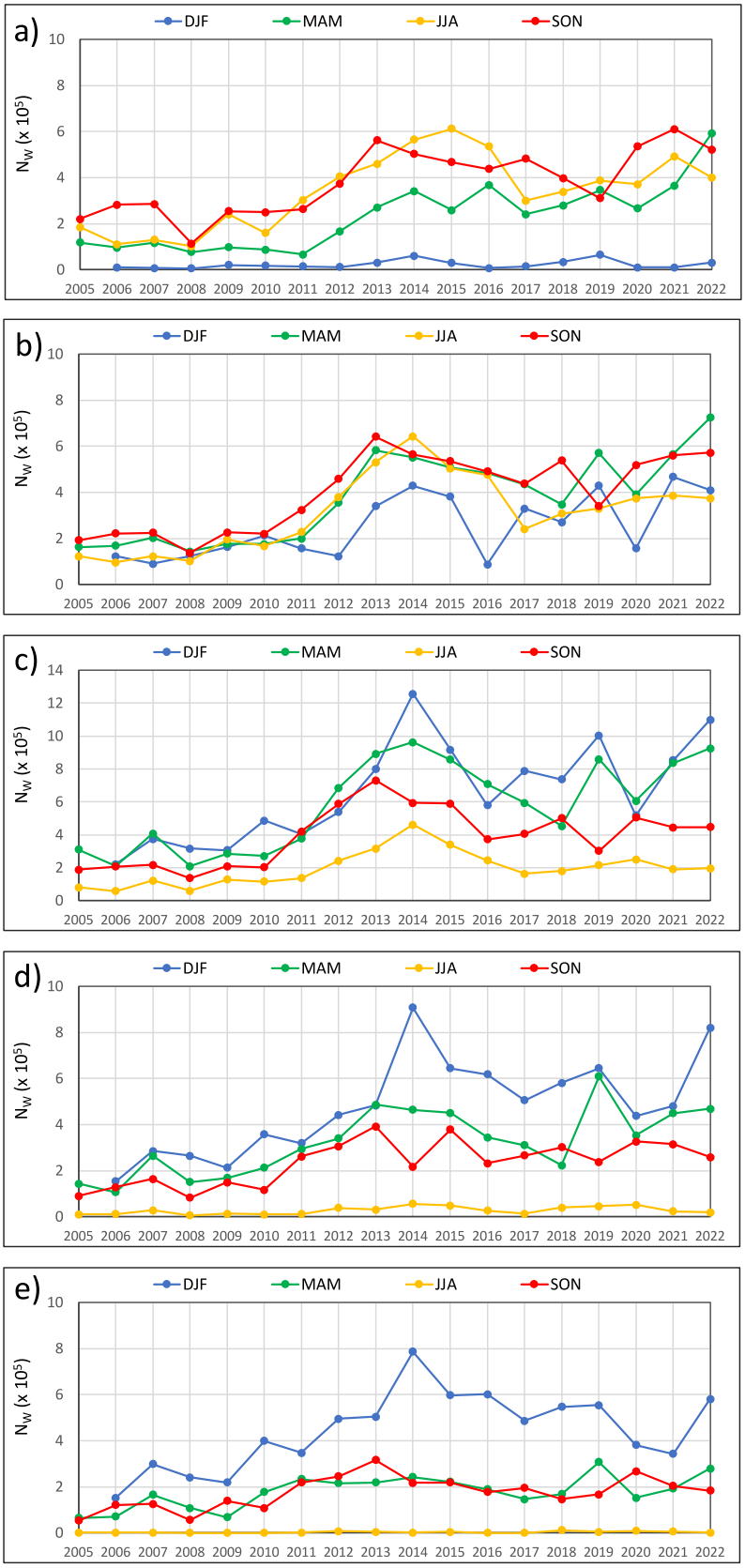

Fig. 9. Number of flashes from WWLLN for each season within each zonal band: (a) N2, (b) N1, (c) S1, (d) S2 and (e) S3. The first complete season is MAM in 2005.

Table 3
Small areas where the maximum of flash proportion is located for each season during a period of 2005–2013 and the value of the flash proportion (related to the annual activity).

Year Season	2005	2006	2007	2008	2009	2010	2011	2012	2013
DJF		#13	#13	#13	#12	#14	#14	#14	#14
		2.85%	2.53%	3.50%	2.42%	4.38%	2.38%	2.91%	2.43%
MAM	#12	#11	#11	#11	#11	#14	#11	#11	#11
	3.45%	2.85%	3.68%	2.67%	2.73%	2.13%	2.37%	2.96%	2.56%
JJA	#3	#8	#13	#9	#1	#7	#4	#2	#8
	1.84%	1.30%	1.61%	1.19%	1.82%	1.23%	1.67%	1.65%	1.81%
SON	#13	#3	#3	#13	#14	#3	#14	#14	#14
	2.48%	2.85%	2.23%	1.62%	2.16%	1.93%	2.55%	3.16%	2.89%

Table 4
Same as in Table 3 for the period of 2014–2022.

Year Season	2014	2015	2016	2017	2018	2019	2020	2021	2022
DJF	#14	#14	#14	#13	#13	#13	#12	#12/#13	#13
	3.90%	4.02%	2.92%	3.31%	3.47%	3.74%	2.01%	2.6%	3.29%
MAM	#14	#14	#14	#11	#14	#11	#11	#12	#12
	2.6%	2.8%	2.82%	2.6%	1.98%	3.46%	2.59%	3.12%	3.2%
JJA	#8	#8	#8	#2	#4	#8	#7	#7	#7
	2.23%	2.14%	2.0%	1.11%	1.39%	1.47%	1.74%	1.52%	1.33%
SON	#14	#14	#8	#3	#13	#7	#13	#3	#7
	2.02%	2.5%	1.72%	1.99%	2.38%	1.29%	2.15%	2.02%	1.69%

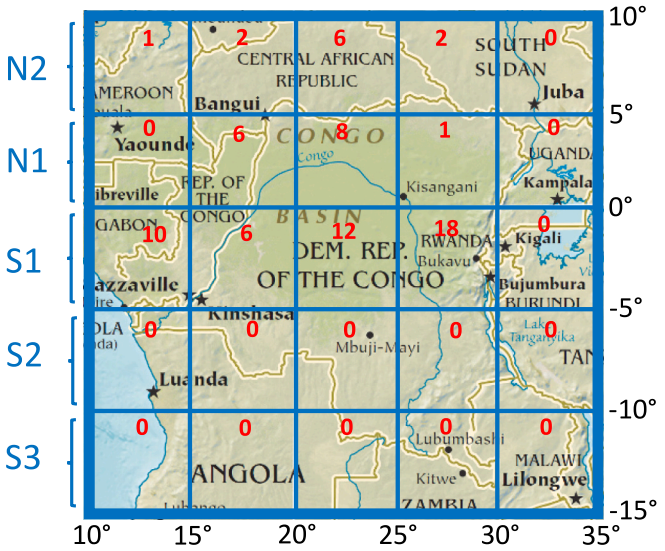

Fig. 10. Number of times (red numbers) with the seasonal maximum for each small area during the 18 years period (71 complete seasons including one season with two areas evenly matched leading to a total of 72). (For interpretation of the references to color in this figure legend, the reader is referred to the web version of this article.)

of the lightning activity found in our study area using LIS and in Qie et al. (2020), for example a peak in 2009. The year 2013 corresponds with a long sequence of low values of the Oceanic Niño Index (ONI) according to the Climate Prevision Center (CPC)[1] of the National Oceanic and Atmospheric Administration (NOAA). The ONI, which is one measure of the El Niño-Southern Oscillation, indicates negative values (i.e., La Niña episode) from May–July in 2010 to March–May in 2012, neutral values from April–June in 2012 to August–October in 2014 and then a significant El Niño episode from September–November in 2014 to March–May in 2016 with a maximum value around the end of 2015 and the beginning of 2016. The year 2016 was the hottest year in the world before being dethroned by 2023. Actually, we do not see any significant correlation between the lightning activity and the ONI.

The period around 2013 corresponds also with a maximum in the solar activity as shown for example in Bhowmik and Nandy (2018). Indeed, their Fig. 4 showed a maximum in the 24th sunspot cycle around 2013 but the observed maximum peaks at 2014. On the contrary, for the lightning activity in 2014, the LIS data shows a decrease while the WWLLN data shows a moderate increase of the flash number associated with a large increase of the multiplicity. Thus, there is no direct relationship between lightning and solar activities. This kind of correlation is still in debate as noted in Scott et al. (2014) who analyzed the effect of the solar wind on lightning. Holzworth et al. (2019) showed that a net maximum of lightning superbolts in 2014 is well correlated with the maximum of the 24th sunspot cycle. However, the superbolts were mainly detected over seas and oceans where the lightning activity is well known to be low, not in the regions with strong lightning activity (i.e., the lightning "chimneys"). The present study is on the contrary focused on the most active region of the Earth.

At the scale of the zonal bands, we can observe characteristics of flash proportion along the period as it is shown by Fig. 6. The two most northern bands, both in the north hemisphere, exhibit a proportionally-increasing trend, while the first band below the equator tends to stay constant (the largest proportion of about 30%), and the two most southern bands have a decreasing trend. The two most fluctuanting proportions, which are also the lowest, are in the most northern and southern bands, N2 and S3, respectively. The variability is larger at the scale of the small areas, especially in the most active zonal band, i.e., S1. Indeed, if the annual maximum of the flash proportion is by far always in the same band S1, it is not constantly in the same small area. Thus, it is chronologically in area #13 (4 years), area #14 (8 years), area #13 (3 years), area #12 (3 years) with the maximum value in area #14 with 10.4% in 2015 (Fig. 7h). However, the density maximum at high resolution is always in area #14 which corresponds with the major maximum in Kigotsi et al. (2018). The contrast between the major and the secondary maximum increases more to the west in the period of 2005–2014 and then decreases substantially (Fig. 4). Finally, the

[1] https://origin.cpc.ncep.noaa.gov/products/analysis_monitoring/ensostuff/ONI_v5.php

average proportion of flashes is slightly larger in area #13 compared to area #14 (7.96% vs. 7.81%, Fig. 5). Previous works highlighted the specificity of the areas #13 and #14: there are more MCSs in area #14 than in area #13, on the contrary there are more flashes per MCS in area #13 than in area #14, i.e. thunderstorms are more active in area #13 than in area #14 (Jackson et al., 2009).

Various factors can influence the spatial distribution of flashes in the study area. The most determining, at the scale of the 5° wide zonal bands, are undoubtedly the migratory cycle of the intertropical convergence zone (ITCZ) and the seasonality of the equatorial atmospheric waves of Kelvin and of the East African jet AEJ-S (Nguyen and Duvel, 2008; Jackson et al., 2009; Laing et al., 2011). At lower scales, there are other miscellaneous factors such as maximum convergence, maximum wind shear, movement and regeneration of MCSs as well as surface characteristics such as topography or the presence of lakes (Soula et al., 2016; Jackson et al., 2009; Laing et al., 2011). The features seen in DJF and JJA correspond, in fact, to the lower values of the sun's elevation in the northern hemisphere and the southern hemisphere, respectively (Jackson et al., 2009; Ba and Nicholson, 1998): lightning proportions are greater in south of the equator during DJF while during JJA, they are larger in north of the equator (Fig.s 8 and 9). Finally, the seasonal maximum proportion of flashes at the scale of the small areas occurs for a large majority of times (65%) in one of the band S1, but can also occur in the northern bands (N1 and N2) as shown in Tables 3 and 4. During MAM, it occurs 10 times in area #11, which is the majority prior to areas #14 and #12 with 5 and 3 times, respectively. During SON, the activity is less westerly propagated because the maximum occurrence of the proportion is farther scattered over 5 small areas (#14, #13, #3, #8 and #7). The difference in MAM and SON could be explained by the the influence of coupled equatorial Kelvin waves or the Eastern African Jet from the Southern Hemisphere (AEJ-S). Indeed, Kelvin waves are more frequent and it can modulate the convection activity in equatorial Africa during MAM (Laing et al., 2011; Nicholson and Grist, 2003). On the other hand, the AEJ-S jet is well developed in equatorial Africa during SON, while it is practically absent during MAM (Jackson et al., 2009, Nicholson and Grist, 2003). The frequent occurrence of flash proportion peaks in area #11 during MAM is consistent with some results of Laing et al. (2011). They actually found that the peak of convection covers the western sector of equatorial Africa during the peak of the wet phase of the Kelvin waves, during which Outgoing Longwave Radiation (OLR) anomalies bring moisture from the Gulf of Guinea to the convergence zones of the lower layers of the atmosphere at 850 hPa, in equatorial Africa (Laing et al., 2011). But since wind shear can be observed in the center of the DRC during MAM (Jackson et al., 2009) and since deep convection is often associated with the maxima of this shear in the 925–600 hPa layer of the troposphere (Laing et al., 2008; Mohr and Thorncroft, 2006), it is also possible that MCSs develop in the area #13 and/or area #12 and then move westward to area #11 where they contribute to these peaks.

The organization of MCS is dictated by synoptic conditions at upper and lower levels (Maddox, 1980). Thus, the convective intensification shown in Kigotsi et al. (2022) with the MCS development in the night of March 04, 2013, which became stationary in the area #14 and then moved to over the Virunga mountains as a tiny thunderstorm cell, illustrates low-level convergence conditions in the main maximum area. Similarly, the life cycle of a stationary MCS observed in the same area #14 on December 25, 2013, described in Kigotsi et al. (2022), which first involved the merger of several cells and the regenerations before its development, illustrates the property of this convergence zone. However, other thunderstorm systems can develop farther in the west of the same latitude level during DJF and can cover large regions with longer lifetimes (Kigotsi et al., 2022), which explains the possible locations of the maximum proportion in the areas #14, #13 and #12 during different seasons. In the same zonal band (S1), the area #15 exhibits a specific thunderstorm activity mainly located over Lake Victoria, with very low flash proportion during all JJA (< 0.5%) and high fluctuation during DJF, with for example a very low value in 2005 and a constant increase during the last five years up to about 3%. This convective activity over Lake Victoria, east of the Virunga Mountains, is associated with nocturnal thermodynamic conditions involving the combined effects of lake and mountain-valley breezes (Fraedrich, 1972; Laing et al., 2011).

It is instructive to associate the small areas defined in the present study and the locations of the high densities highlighted on a planetary scale in previous works (Christian et al., 2003; Albrecht et al., 2016). The result is presented in Table 5. In the global climatology of Christian et al. (2003) performed with a resolution of 0.5°, the four largest densities of lightning in the world are located in the DRC and the maximum planetary density (1.25°S, 27.75°E), which is in the DRC (not in Rwanda as the authors wrote). They also identified three other sites associated with high localized densities: Boende1, Kananga and Lusambo. The coordinates of these sites and the corresponding small areas are shown in Table 5. The study of Albrecht et al. (2016) showed the locations of high densities of lightning by continent at a high resolution of 0.1°. It ranks the sites of Kabare (205.31 flashes km^{-2} yr^{-1}) and Kampene (176.71 flashes km^{-2} yr^{-1}) for the second and third largest densities in the world, respectively, after the region of Lake Maracaibo, in Venezuela (232.52 flashes km^{-2} yr^{-1}). It also ranks Sake, Butembo and Boende2 among the ten largest local densities in the world. Even Boende3, Kindu and Kisangani appear among the twenty largest flash densities in the world in Albrecht et al. (2016). The coordinates of all these 12 sites are shown in Table 5 with the corresponding small areas. They are on the DRC territory and associated with five different small areas, especially with the area #14 for 5 of them. In fact, the proximity of 11 of them defines a square (areas #8, #9, #13 and #14) which corresponds to the maximum density observed in the eastern part of the DRC (Soula et al., 2016).

5. Conclusion

The total lightning activity within the Congo Basin issued from the WWLLN is analyzed during a period of 18 years between 2005 and 2022, which extends from the previous studies with the half term, i.e., between 2005 and 2013. The 18–year period allows an examination of the trend in the lightning occurrences in a wide and active region of the Earth, in a context of strong global warming, in particular over the latest 8 years. The lightning flashes provided by LIS on board the TRMM between 2005 and 2014 and the ISS between 2018 and 2022 complete the dataset for the study. The methodology consists first in a reconstruction of flashes from strokes detected by the WWLLN and a calculation of several annual parameters thanks to these flashes: the flash number, the average multiplicity, the maximum of the flash density at a resolution of 0.1° × 0.1°, the detection efficiency (DE_W) of WWLLN relative to LIS (the total flash from LIS has been estimated by considering the coefficient of the coverage of the study domain). Then, the lightning activity in terms of flash number and proportion is analyzed at various spatial (zonal bands and small areas of 5° × 5°) and temporal (year and season) scales.

Table 5
Location of the maximum lightning densities documented in the literature.

Location name	Reference	Latitude	Longitude	Areas
Earth maximum	Christian et al. (2003)	1.25°S	27.75°E	#14
Boende1	Christian et al. (2003)	0.25°N	20.75°E	#8
Kananga	Christian et al. (2003)	5 0.75°S	18.75°E	#17
Lusambo	Christian et al. (2003)	4.75°S	24.25°E	#13
Kabare	Albrecht et al. (2016)	1.85°S	27.75°E	#14
Kampene	Albrecht et al. (2016)	3.05°S	27.65°E	#14
Sake	Albrecht et al. (2016)	0.95°N	27.95°E	#14
Butembo	Albrecht et al. (2016)	0 0.25°N	28.45°E	#9
Boende2	Albrecht et al. (2016)	1.55°S	20.95°E	#13
Boende3	Albrecht et al. (2016)	0.55°N	20.35°E	#8
Kindu	Albrecht et al. (2016)	2.45°S	26.95°E	#14
Kisangani	Albrecht et al. (2016)	0.35°N	26.65°E	#9

The major results at annual scale can be summarized as follows: (i) a marked interannual evolution of the lightning activity is observed in the entire study region; (ii) the number of lightning flashes is strongly correlated with the average multiplicity at various scales of space, which suggests that its changes are mainly explained by variations in DE_W; (iii) the local maximum density of flashes is always in the same 5° × 5° area (#14) during the 18–year period; (iv) annual proportions of the lightning activity in the 5° latitude zonal bands show various trends: increasing trend in the two bands north of the equator, constant most activity in the band just below the equator, and decreasing trend in the two furthest south zones from the equator.

At more local scales and for the classic seasons, signatures associated with the migration cycle of the ITCZ are clearly highlighted and some seasonal singularities can be interpreted by evoking the role of factors such as Kelvin waves or the AEJ-S jet: (i) each year, the proportions of lightning flashes are almost zero in the zonal bands (5–10°N) and (10–15°S) during DJF and JJA, respectively; (ii) the maximum proportion of lightning at the scale of the small areas (5° × 5°) is found in the first southern zonal band (between 0° and 5°S) entirely on the annual scale and in 65% of cases on the seasonal scale; (iii) for the most active season (DJF) and the intermediate one (MAM), the proportion becomes 100%, while it is more scattered for the less active season (JJA) in the two northern zonal bands with 94% of cases.

CRediT authorship contribution statement

Jean Kasereka Kigotsi: Writing – review & editing, Writing – original draft, Visualization, Validation, Software, Methodology, Investigation, Conceptualization. **Serge Soula:** Writing – review & editing, Writing – original draft, Visualization, Validation, Supervision, Methodology, Investigation, Formal analysis, Conceptualization. **Gilles Athier:** Writing – review & editing, Validation, Software, Methodology. **Louis Kongoda Lisika:** Writing – review & editing, Validation, Software. **Keun-Ok Lee:** Writing – review & editing, Validation, Methodology, Data curation.

Declaration of competing interest

The authors declare that they have no known competing financial interests or personal relationships that could have appeared to influence the work reported in this paper.

Data availability

Data will be made available on request.

Acknowledgements

The authors thank the World Wide Lightning Location Network (http://wwlln.net/) for providing the lightning location data used in this study. They are grateful to US National Aeronautics and Space Administration (NASA) and Global Hydrology Resource Center (GHRC) for LIS data available on their website.

Reference

Abarca, S.F., Corbosiero, K.L., 2011. The World Wide Lightning Location Network and convective activity in tropical cyclones. Mon. Weather Rev. 139, 175–191.

Abarca, S.F., Corbosiero, K.L., Galarneau, T.J., 2010. An evaluation of the Worldwide Lightning Location Network (WWLLN) using the National Lightning Detection Network (NLDN) as ground truth. J. Geophys. Res. 115, D18206 https://doi.org/10.1029/2009JD013411.

Albrecht, R.I., Goodman, S.J., Petersen, W.A., Buechler, D.E., Bruning, E.C., Blakeslee, R. J., Christian, H.J., 2011. The 13 years of TRMM Lightning Imaging Sensor: from individual flash characteristics to decadal tendencies. In: Proceedings of the XIV International Conference on Atmospheric Electricity, 08–12 August 2011. Brazil, Rio de Janeiro.

Albrecht, R., Goodman, S., Buechler, D., Blakeslee, R., Christian, H., 2016. Where are the lightning hotspots on Earth? Bull. Amer. Meteor. Soc. 97, 2051–2068. https://doi.org/10.1175/bams-d-14-00193.1.

Altaratz, O., Koren, I., Yair, Y., Price, C., 2010. Lightning response to smoke from Amazonian fires. Geophys. Res. Lett. 37, L07801 https://doi.org/10.1029/2010GL042679.

Antonescu, B., Burcea, S., 2010. A cloud-to-ground lightning climatology for Romania. Mon. Weather Rev. 138, 579–591. https://doi.org/10.1175/2009MWR2975.1.

Ba, M.B., Nicholson, S.E., 1998. Analysis of convective activity and its relationship to the rainfall over the Rift Valley Lakes of east Africa during 1983–90 using the Meteosat infrared channel. J. Appl. Meteorol. 37, 1250–1264.

Bhowmik, P., Nandy, D., 2018. Prediction of the strength and timing of sunspot cycle 25 reveal decadal-scale space environmental conditions. Nat. Commun. 9, 5209. https://doi.org/10.1038/s41467-018-07690-01234567890.

Blakeslee, R.J., Lang, T.J., Koshak, W.J., Buechler, D., Gatlin, P., Mach, D.M., et al., 2020. Three years of the Lightning Imaging Sensor onboard the International Space Station: Expanded global coverage and enhanced applications. J. Geophys. Res.-Atmos. 125 https://doi.org/10.1029/2020JD032918 e2020JD032918.

Boccippio, D.J., Koshak, W.J., Blakeslee, R.J., 2002. Performance Assessment of the Optical Transient Detector and Lightning Imaging Sensor. Part I: Predicted Diurnal Variability. J. Atmos. Ocean. Technol. 19, 1318–1332.

Bovalo, C., Barthe, C., Begue, N., 2012. A lightning climatology of the South-West Indian Ocean. Nat. Hazards Earth Syst. Sci. 12, 2659–2670. https://doi.org/10.5194/nhess-12-2659-2012.

Burgesser, R.E., Nicora, M.G., Avila, E.E., 2012. Characterization of the lightning activity of ''Relampago del Catatumbo''. J. Atmos. Sol. Terr. Phys. 77, 241–247. https://doi.org/10.1016/j.jastp.2012.01.013.

Cecil, D., Buechler, D.E., Blakeslee, R.J., 2014. Gridded lightning climatology from TRMM-LIS and OTD: Dataset description. Atmos. Res. 135, 404–414. https://doi.org/10.1016/j.atmosres.2014.06.028.

Christian, H.J., Blakeslee, R.J., Goodman, S.J., Mach, D.A., Stewart, M.F., Buechler, D.E., Koshak, W.J., Hall, J.M., Boeck, W.L., Driscoll, K.T., Boccippio, D.J., 1999. The Lightning Imaging Sensor. In: Proceedings of the 11th International Conference on Atmospheric Electricity, Huntsville, AL, NASA, pp. 746–749.

Christian, H.J., Blakeslee, R.J., Boccippio, D.J., Boeck, W.L., Buechler, D.E., Driscoll, K. T., Goodman, S.J., Hall, J.M., Koshak, W.J., Mach, D.M., Stewart, M.F., 2003. Global frequency and distribution of lightning as observed from space by the Optical Transient Detector. J. Geophys. Res. 108 (D1), 4005. https://doi.org/10.1029/2002JD002347.

DeMaria, M., DeMaria, R.T., Knaff, J.A., Molenar, D., 2012. Tropical cyclone lightning and rapid intensity change. Mon. Weather Rev. 140, 1828–1842. https://doi.org/10.1175/MWR-D-11-00236.1.

Dowden, R.L., Brundell, J.B., Rodger, C.J., 2002. VLF lightning location by time of group arrival (TOGA) at multiple sites. J. Atmos. Solar-Terr. Phys. 64, 817–830.

Fraedrich, K., 1972. A simple climatological model for the dynamics and energetics of the nocturnal circulation at Lake Victoria. Q. J. R. Meteorol. Soc. 98, 322–335.

Hodanish, S., Sharp, D., Collins, W., Paxton, C., Orville, R., 1997. A 10-yr monthly lightning climatology of Florida: 1986–95. Weather Forecast. 12, 439–448.

Holzworth, R.H., McCarthy, M.P., Brundell, J.B., Jacobson, A.R., Rodger, C.J., 2019. Global distribution of superbolts. J. Geophys. Res.-Atmos. 124 (9996–10), 005. https://doi.org/10.1029/2019JD030975.

Jackson, B., Nicholson, S., Klotter, D., 2009. Mesoscale convective systems over western equatorial Africa and their relationship to large-scale circulation. Mon. Weather Rev. 137, 1272–1294. https://doi.org/10.1175/2008MWR2525.1.

Kaplan, J.O., Lau, K.H.-K., 2021. The WGLC global gridded lightning climatology and time series. Earth Syst. Sci. Data 13, 3219–3237. https://doi.org/10.5194/essd-13-3219-2021.

Kigotsi, J.K., Soula, S., Georgis, J.F., 2018. Comparison of lightning activity in the two most active areas of the Congo Basin. Nat. Hazards Earth Syst. Sci. 18 (479–489), 2018 doi: org/10.5194/nhess-18-479-2018.

Kigotsi, J.K., Soula, S., Kazadi, A.B.M., Zana, A.N., 2022. Contribution to the study of thunderstorms in the Congo Basin: Analysis of periods with intense activity. Atmos. Res. 269, 106013 doi: org/10.1016/j.atmosres.2021.106013.

Laing, A.G., Carbone, R.E., Levizzani, V., Tuttle, J.D., 2008. The propagation and diurnal cycles of deep convection in northern tropical Africa. Quart. J. Roy. Soc. 134, 93–109.

Laing, A.G., Carbone, R.E., Levizzani, V., 2011. Cycles and propagation of deep convection over equatorial Africa. Mon. Weather Rev. 129, 2832–2853.

Maddox, R.A., 1980. Mesoscale convective complexes. Bull. Amer. Meteor. Soc. 61, 1374–1387 doi:10.1175/1520-0477(1980)061<1374:MCC>2.0.CO;2.

Mohr, K.I., Thorncroft, C.D., 2006. Intense Convective Systems in West Africa and their relationship to the African easterly jet. Quart.J.Roy.Meteor.Soc. 132, 163–176.

Nguyen, H., Duvel, J.-P., 2008. Synoptic wave perturbations and convective systems over equatorial Africa. J. Clim. 21, 6372–6388.

Nicholson, S., Grist, J.P., 2003. On the seasonal evolution of atmospheric circulation over West Africa and equatorial Africa. J. Clim. 16, 1013–1030.

Oki, T., Musiake, K., 1994. Seasonal change of the diurnal cycle of precipitation over Japan and Malaysia. J. Appl. Meteorol. 33, 1445–1463.

Pujol, O., Georgis, J., Chong, M., Roux, F., 2005. Dynamics and microphysics of orographic precipitation during MAP-IOP3. Q. J. R. Meteorol. Soc. 131, 2795–2819.

Qie, K., Tian, W., Wang, W., Wu, X., Yuan, T., Tian, H., et al., 2020. Regional trends of lightning activity in the tropics and subtropics. Atmos. Res. 242, 104960 https://doi.org/10.1016/j.atmosres.2020.104960.

Qie, K., Qie, X., Tian, W., 2021. Increasing trend of lightning activity in the South Asia region. Sci. Bull. 66 (1), 78–84. https://doi.org/10.1016/j.scib.2020.08.033.

Qie, X., Qie, K., Wei, L., Zhu, K., Sun, Z., Yuan, S., et al., 2022. Significantly increased lightning activity over the Tibetan Plateau and its relation to thunderstorm genesis. Geophys. Res. Lett. 49 https://doi.org/10.1029/2022GL099894 e2022GL099894.

Rodger, C.J., Brundell, J.B., Holzworth, R.H., Lay, E.H., 2008. Growing detection efficiency of the World Wide Lightning Location Network. Am. Inst. Phys. Conf. Proc., Coupling of Thunderstorms and Lightning Discharges to Near-Earth Space: Proceedings of the Workshop, Corte (France), 23–27 June 2008. 1118, 15–20. https://doi.org/10.1063/1.3137706.

Rudlosky, S.D., Shea, D.T., 2013. Evaluating WWLLN performance relative to TRMM/LIS. Geophys. Res. Lett. 40, 2344–2348.

Scott, C.J., et al., 2014. Evidence for solar wind modulation of lightning. Environ. Res. Lett. 9, 055004 https://doi.org/10.1088/1748-9326/9/5/055004.

Soula, S., van der Velde, O.A., Montanya, J., Huet, P., Barthe, C., Bór, J., 2011. Gigantic Jets produced by an isolated tropical thunderstorm near Réunion Island. J. Geophys. Res. 116, D19103 https://doi.org/10.1029/2010JD015581.

Soula, S., Kigotsi, K.J., Georgis, J.F., Barthe, C., 2016. Lightning climatology in the Congo Basin. Atmos. Res. 178–179, 304–319. https://doi.org/10.1016/j.atmosres.2016.04.006.

Wheeler, M., Kiladis, G.N., 1999. Convectively coupled equatorial waves : analysis of clouds and temperature in the wavenumber-frequency domain. J. Atmos. Sci. 56, 374–399.

Wheeler, M., Kiladis, G.N., Webster, P.J., 2000. Large-scale dynamical fields associated with convectively coupled equatorial waves. J. Atmos. Sci. 57, 613–640.

Williams, E., Stanfill, S., 2002. The physical origin of the land–ocean contrast in lightning activity. C.R. Phys. 3, 1277–1292. https://doi.org/10.1016/S1631-0705(02)01407-X.

World Meteorological Organization, 2023. WMO annual report highlights continuous advance of climate change https://public.wmo.int/en/media/press-release/wmo-annual-report-highlights-continuous-advance-of-climate-change.

Yang, G.Y., Slingo, J., 2001. The diurnal cycle in the Tropics. Mon. Weather Rev. 129, 784–801.